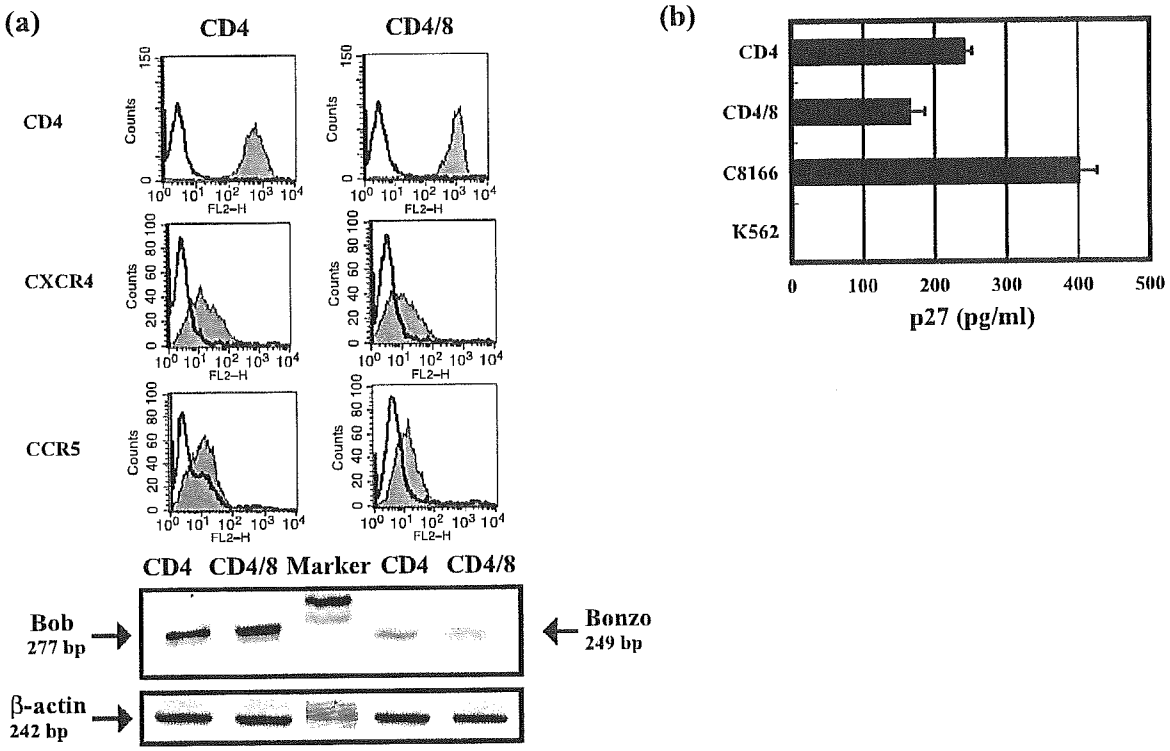

Fig. 4. Expression of receptor and co-receptor on $CD4^+$ and $CD4^+8^+$ T cells. **a** Uninfected cells were stained with PE-labeled anti-CD4 mAb, PE-labeled anti-CXCR4 mAb, or PE-labeled anti-CCR5 mAb, followed by propidium iodide staining to exclude dead cells. RNA was isolated from uninfected cells and then reverse-transcribed into cDNA. cDNA was subjected to semi-quantitative PCR using Bob, Bonso or β-actin primer. The thermal cycle consisted of 30 s at 94 °C, 45 s at 52 °C for Bob, 58 °C for Bonso or 55 °C for β-actin, 45 s at 72 °C. The numbers of PCR cycles for Bob and Bonso were 35 cycles, and those for β-actin were 24 cycles to generate PCR products during the exponential phase of amplification. **b** Entry efficiency of virus into $CD4^+$ and $CD4^+8^+$ T cells. Cells were incubated with virus (moi 1) for 2 h, followed by washing, trypsinizing, and lysed with lysis buffer. The p27 core antigen content in the lysate was monitored by ELISA. C8166 cells were used as positive control and K562 cells were used as negative one. The data shown are the mean of triplicate cultures ±SD

in $CD4^+8^+$ T cells (Fig. 4a). When we monitored the efficiency of virus entry into $CD4^+$ and $CD4^+8^+$ T cells at 2 h post-infection by the measurement of the intracellular p27 antigens, a slightly lower level of the amount of p27 antigens in $CD4^+8^+$ T cells was observed when compared with $CD4^+$ T cells (Fig. 4b). These observations indicate that the entry step of virus did not account for the increased amounts of virus accumulation in $CD4^+8^+$ T cells.

Efficiency of reverse transcription in $CD4^+$ and $CD4^+8^+$ T cells

To define at which step virus replication is accelerated in $CD4^+8^+$ T cells, we performed DNA-dependent PCR with primers that distinguish salient stages of

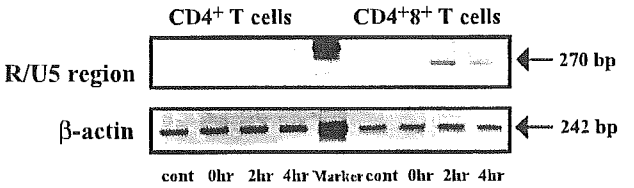

Fig. 5. Detection of the earliest reverse transcription product of SIV in $CD4^+$ and $CD4^+8^+$ T cells. DNA was isolated from infected or uninfected cells at indicated time and subjected to semi-quantitative PCR using R/U5 or β-actin primer. The thermal cycle consisted of 30 s at 94 °C, 45 s at 64 °C for R/U5 and 55 °C for β-actin, 45 s at 72 °C. The numbers of PCR cycles for R/U5 were 35 cycles, and those for β-actin were 25 cycles to generate PCR products during the exponential phase of amplification

reverse transcription. Cells were infected with SIV (moi 1) for 2 h. After washing to remove free virus, cells were further cultured and the genomic DNA was extracted from infected cells at 0, 2, and 4 h after incubation. The primer pair R/U5 can amplify the earliest reverse transcription product [1]. This earliest reverse transcription product was detected in both $CD4^+$ T cells and $CD4^+8^+$ T cells at 2 h after incubation, however, level of the product was higher in $CD4^+8^+$ T cells than in $CD4^+$ T cells (Fig. 5). Thus, after the entry of SIV, reverse transcription appeared to initiate more efficiently in $CD4^+8^+$ T cells than in $CD4^+$ T cells.

We speculated that some cellular components might act to function as an inhibitor or cofactor for viral reverse transcriptase in cells. We thus prepared the cell lysate from uninfected $CD4^+$ T cells or $CD4^+8^+$ T cells and performed RT assay in the presence of those cell lysate. In all cases, RT activity was decreased in the presence of cell lysate from both types of T cells, however, the lysate from $CD4^+$ T cells impaired the RT activity more strongly than that from $CD4^+8^+$ T cells (Table 1). These results indicate that $CD4^+8^+$ T cells possess a favorable environment for intracellular reverse transcription.

Table 1. Effect of cell lysates on RT activity

RT source	Cell lysates			
	$CD4^+$T cells	$CD4^+8^+$ T cells	No lysates	p value[c]
SIVmac239	332 ± 15[a]	765 ± 158	1665 ± 271	$p < 0.05$
SHIV3rN	802 ± 75	1086 ± 98	9346 ± 1883	$p < 0.05$
M-MLV-RT[b]	17039 ± 1218	53211 ± 1619	100713 ± 13490	$p < 0.01$

Cell lysates were prepared from $CD4^+$ and $CD4^+8^+$ T cells. RT assay was performed in the presence or absence of cell lysates

[a] cpm/10 μg protein

[b] Moloney Murine Leukemia Virus Reverse Transcriptase (Gibco): 8.3 U

[c] $CD4^+$ T cells versus $CD4^+8^+$ T cells

Discussion

We observed in this study that SIV replicated more efficiently in $CD4^+8^+$ T cells than in $CD4^+$ T cells, of which expression levels of receptors and turnover rate were almost the same. We therefore set out to focus at which steps SIV replication was accelerated in $CD4^+8^+$ T cells. We found that reverse transcription initiated more efficiently in $CD4^+8^+$ T cells than in $CD4^+$ T cells. Therefore, we presumed that intracellular environment in $CD4^+8^+$ T cells was optimal for reverse transcription. After the entry of virus, productive HIV-1/SIV infection requires overcoming several cellular blocks in the establishment of provirus and its replication. There have been significant advances in the identification of cellular cofactors that affect events in HIV-1 replication after entry of virus [23]. Kinoshita et al. demonstrated that a nuclear factor of activated T cells (NFAT) overcame a blockade at reverse transcription and permitted active HIV-1 replication [13]. Although the target genes for NFAT that can aid completed reverse transcription are unknown, NFAT appears to be involved in HIV-1 replication at pre- and post integrative steps of the HIV-1 life cycle. Although we have not yet determined whether NFAT expression was more greatly enhanced in $CD4^+8^+$ T cells, it is possible that $CD4^+8^+$ T cells contain either known or unknown factors that permit reverse transcription like NFAT, or fewer cellular factors that inhibit reverse transcription.

Many investigators have provided evidence for the widespread infection of CD8 T cells by HIV-1/SIV both in vitro and in vivo [5, 10]. In most cases, transient co-expression of CD4 during maturation or activation renders them susceptible to HIV-1/SIV infection and destruction [14, 29]. In our case, the efficiency of virus entry into $CD4^+8^+$ T cells was almost the same as into $CD4^+$ T cells. An important issue is whether the expression of CD8 molecules on $CD4^+8^+$ T cells is related to induce a higher permissive state for virus replication. To solve this question, we are currently designing the experiment using CD8 specific RNAi which offers a valuable opportunity to modulate the expression of cellular genes.

We have established $CD4^+8^+$ T cells and $CD4^+$ T cells from rhesus macaque PBMC. $CD4^+8^+$ T cells in PBMC are observed in approximately 3% of human and 5% of rhesus macaques [11, 22]. Several reports have shown that activation of $CD8^+$ T cells from peripheral blood resulted in the de novo expression of CD4 molecule and these peripheral $CD4^+8^+$ T cells were in the activated states [2, 14, 24]. Also, it has been reported that the majority of the intestinal T cells including $CD4^+8^+$ T cells are memory T cells and are in an activated state [12]. Since HIV-1/SIV is assumed to preferentially infect and kill the activated T cells [28], $CD4^+8^+$ T cells in the peripheral blood or the intestine may be readily infected by the virus and produce a large amount of virus. The high level of viral production disseminates infection systemically and provides access to large numbers of target cells for prolonged replication. The function of $CD4^+8^+$ T cell subset in these organs is not fully defined, however, we speculate that infected $CD4^+8^+$ T cells might play an important role for early viral dissemination and

serve as a potent viral reservoir in HIV-1/SIV infection. On the other hand, we observed that the number of viable cells in infected $CD4^+$ T cells were considerably more than that in infected $CD4^+8^+$ T cells, which indicated that the depletion of $CD4^+$ T cells by SIV infection were less. Previous studies have also shown that the depletion of $CD4^+$ T cells in PBMC was gradual in HIV-1/SIV infection [11]. The low level of viral replication could provide a mechanism for cells to escape the host defense surveillance and favor establishment of a persistent infection. Therefore, although there were little differences between $CD4^+$ T cells and $CD4^+8^+$ T cells in the expression level of receptors, both types of CD4 positive cells might play distinct roles in HIV-1/SIV infection.

In the present study, we compared the susceptibility to SIV infection in $CD4^+$ T cells and $CD4^+8^+$ T cells using HVS-transformed T cell lines. Although we have not confirmed our findings by ex vivo analysis using PBMC from rhesus macaques, our model may be helpful in understanding the viral replication and reservoirs in vivo.

Acknowledgments

We thank Dr. M. Yasukawa for generously providing the 488 strain of H. saimiri group C.

References

1. Akahata W, Ido E, Hayami M (2003) Mutational analysis of two zinc finger motifs in the nucleocapsid protein of SIVmac239. J Gen Virol 84: 1641–1648
2. Blue ML, Daley JF, Levine H, Craig KA, Schlossman SF (1986) Biosynthesis and surface expression of T8 by peripheral blood $T4^+$ cells in vitro. J Immunol 137: 1202–1207
3. Calabro ML, Zanotto C, Calderazzo F, Crivellaro C, Mistro AD, Rossi AD, Chieco-Bianchi L (1995) HIV-1 infection of the thymus: evidence for a cytopathic and thymotropic viral variant in vivo. AIDS Res Hum Retrovir 11: 11–19
4. Calabro ML, Zanotto C, Calderazzo F, Crivellaro C, Mistro AD, Rossi AD, Chieco-Bianchi L (1995) HIV-1 infection of the thymus: evidence for a cytopathic and thymotropic viral variant in vivo. AIDS Res Hum Retrovir 11: 11–19
5. Dean GA, Reubel GH, Pedersen NC (1996) Simian immunodeficiency virus infection of $CD8^+$ lymphocytes in vivo. J Virol 70: 5646–5650
6. Deng H, Liu R, Wllmeier W, Choe S, Unutmaz D, Burkhart M, Di Marzio P, Marmon S, Sutton RE, Hill CM, Davis CB, Peiper SC, Schall TJ, Littman DR, Landau NR (1996) Identification of a major co-receptor for primary isolates of HIV-1. Nature 381: 667–678
7. Dusserre N, Dezutter-Dambuyant C, Mallet F, Delorme P, Philit F, Ebersold A, Desgranges C, Thivolet J, Schmitt D (1992) In vitro HIV-1 entry and replication in Langerhans cells may clarify the HIV-1 genome detection by PCR in epidermis of seropositive patients. J Invest Dermatol 99: 89S–102S
8. Feng Y, Broder CC, Kennedy PE, Berger EA (1996) HIV-1 entry cofactor: functional cDNA cloning of a seven-transmembrane, G protein-coupled receptor. Science 272: 872–877
9. Hirsch VM, Sharkey ME, Brown CR, Brichacek B, Goldstein S, Wakefield J, Byrum R, Elkins WR, Hahn BH, Lifson JD, Stevenson M (1998) Vpx is required for dissemination

and pathogenesis of SIVsm Pbj: Evidence of macrophage-dependent viral amplification. Nat Med 4: 1401–1408

10. Imlach S, McBreen S, Shirafuji T, Leen C, Bell JE, Simmonds P (2001) Activated peripheral CD8 lymphocytes express CD4 in vivo and are targets for infection by human immunodeficiency virus type 1. J Virol 75: 11555–11564
11. Jason J, Inge KL (2001) Modulation of CD8 and CD3 by HIV or HIV antigens. Scand J Immunol 53: 259–267
12. Kahn JO, Walker BD (1998) Acute human immunodeficiency virus type 1 infection. N Engl J Med 339: 33–39
13. Kinoshita S, Chen BK, Kaneshima H, Nolan GP (1998) Host control of HIV-1 parasitism in T cells by the nuclear factor of activated T cells. Cell 95: 595–604
14. Kitchen SG, JaForge S, Patel VP, Kitchen CM, Miceli MC, Zack JA (2002) Activation of CD8 T cells induces expression of CD4, which functions as a chemotactic receptor. Blood 99: 207–212
15. Kitchen SG, Jones NR, LaForge S, Whitmire JK, Vu BA, Galic Z, Brooks DG, Brown SJ, Kitchen CMR, Zack JA (2004) CD4 on $CD8^+$ T cells directly enhances effector function and is a target for HIV infection. Proc Natl Acad Sci USA 101: 8727–8732
16. Kumar A, Stipp HL, Sheffer D, Narayan O (1999) Use of herpesvirus saimiri-immortalized macaque $CD4^+$ T cell clones as stimulators and targets for assessment of CTL responses in macaque/AIDS models. J Immunol Methods 230: 47–58
17. Levy JA (1993) Pathogenesis of human immunodeficiency virus infection. Microbiol Rev 57: 183–289
18. Marx PA, Spira AI, Gettie A, Dailey PJ, Veazey RS, Lackner AA, Mahoney CJ, Miller CJ, Claypool LE, Ho DD, Alexander NJ (1996) Progesterone implants enhance SIV vaginal transmission and early virus load. Nat Med 2: 1084–1089
19. Mattapallil JJ, Smit-McBride Z, McChesney M, Dandekar S (1998) Intestinal intraepithelial lymphocytes are primed for gamma interferon and MIP-1β expression and display antiviral cytotoxic activity despite severe $CD4^+$ T-cell depletion in primary simian immunodeficiency virus infection. J Virol 72: 6421–6429
20. Rowland-Jones S (1999) HIV infection: where have all the T cells gone? Lancet 354: 5–7
21. Smit-McBride Z, Mattapallil JJ, McChesney M, Ferrick D, Dandekar S (1998) Gastrointestinal T lymphocytes retain high potential for cytokine responses by have severe $CD4^+$ T-cell depletion at all stages of simian immunodeficiency virus infection compared to peripheral lymphocytes. J Virol 72: 6646–6656
22. Stanley SK, McCune JM, Kaneshima H, Justement JS, Sullivan M, Boone E, Baseler M, Adelsberger J, Bonyhadi M, Orenstien J, Fox CH, Fauci AS (1993) Human immunodeficiency virus infection of the human thymus and disruption of the thymic microenvironment in the SCID-hu mouse. J Exp Med 178: 1151–1163
23. Stevenson M (2003) HIV-1 pathogenesis. Nat Med 9: 853–860
24. Sullivan YB, Landay AL, Zack JA, Kitchen SG, Al-Harthi L (2001) Upregulation of CD4 and $CD8^+$ T cells: CD4dimCD8bright T cells constitute an activated phenotype of $CD8^+$ T cells. Immunology 103: 270–280
25. Takahashi M, Osono E, Nakagawa Y, Wang J, Berzofsky JA, Margulies DH, Takahashi H (2002) Rapid induction of apoptosis in $CD8^+$ HIV-1 envelope-specific murine CTLs by short exposure to antigenic peptide. J Immunol 169: 6588–6593
26. Willey RL, Smith DH, Lasky LA, Theodore TS, Earl PL, Moss B, Capon DJ, Martin MA (1988) In vitro mutagenesis identifies a region within the envelope gene of the human immunodeficiency virus that is critical for infectivity. J Virol 62: 139–147

27. Yasukawa M, Inoue Y, Kimura U, Fujita S (1995) Immortalization of human T cells expressing T-cell receptor gamma delta by herpesvirus saimiri. J Virol 69: 8114–8117
28. Zhang ZQ, Schuler T, Zupancic M, Wietgrefe S, Sraskus KA, Reimann KA, Reinhart TA, Rogan M, Cavert W, Miller CJ, Veazey RS, Notermans D, Little S, Danner SA, Richman DD, Havlir D, Wong J, Jordan HL, Schacker TW, Racz P, Tenner-Racz K, Letvin NL, Wolinsky S, Haase AT (1999) Sexual transmission and propagation of SIV and HIV in resting and activated $CD4^+$ T cells. Science 286: 1353–1357
29. Zloza A, Sullivan YB, Connick E, Landay AL, Al-Harthi L (2003) $CD8^+$ T cells that express CD4 on their surface ($CD4^{dim}CD8^{bright}$ T cells) recognize an antigen-specific target, are detected in vivo, and can be productively infected by T-tropic HIV. Blood 102: 2156–2164

Author's address: Hidemi Takahashi, M.D., PhD., Department of Microbiology and Immunology, Nippon Medical School, 1-1-5, Sendagi, Bunkyo-ku, Tokyo 113-8602, Japan; e-mail: htkuhkai@nms.ac.jp

Available online at www.sciencedirect.com
SCIENCE DIRECT®
Biochemical and Biophysical Research Communications 337 (2005) 452–456
BBRC
www.elsevier.com/locate/ybbrc

Temperature-dependent biosynthesis of glucose monomycolate and its recognition by CD1-restricted T cells

Yutaka Enomoto [a,b], Masahiko Sugita [a,c,*], Isamu Matsunaga [c], Takashi Naka [d], Akimasa Sato [d], Tetsuo Kawashima [a,b], Kazuo Shimizu [b], Hidemi Takahashi [a], Yoshihiko Norose [a], Ikuya Yano [d]

[a] *Department of Microbiology and Immunology, Nippon Medical School, 1-1-5 Sendagi, Bunkyo-ku, Tokyo 113-8602, Japan*
[b] *Department of Surgery, Nippon Medical School, 1-1-5 Sendagi, Bunkyo-ku, Tokyo 113-8602, Japan*
[c] *Laboratory of Cell Regulation, Institute for Virus Research, Kyoto University, 53 Kawahara-cho, Shogoin, Sakyo-ku, Kyoto 606-8507, Japan*
[d] *Japan BCG Central Laboratory, 3-1-5 Matsuyama, Kiyose, Tokyo 204-0022, Japan*

Received 6 September 2005
Available online 21 September 2005

Abstract

Mycolic acids are long chain fatty acids that constitute the lipid-rich cell wall framework of mycobacteria. Upon infection, mycobacteria begin to synthesize glucose monomycolate (GMM), a glucosylated species of mycolic acids, by utilizing host-derived glucose as sugar source. Accordingly, GMM production serves as a good indicator for local invasion of mycobacteria, and its detection by the host immune system would favor efficient monitoring of mycobacterial infection. Here, we found that GMM was produced abundantly at 30 °C rather than at 37 °C and recognized by a GMM-specific, CD1-restricted T cell line that was isolated from mycobacteria-infected human skin. Since the common portal sites for mycobacterial infection include ventilating alveoli of the lung and the externally exposed skin that often render invading microbes survive at reduced temperature, sampling GMM by CD1 lipid antigen-presenting molecules may allow the host to detect mycobacterial infection at its early phases.

Keywords: Mycobacteria; Glucose monomycolate; CD1

The thick cell wall of mycobacteria is unique in that it contains a variety of hydrophobic lipid and glycolipid components [1]. Covalently associated with the underlying arabinogalactan and peptidoglycan layers, mycobacteria-specific fatty acids, termed mycolic acids, are densely aligned with their extremely long carbon chains extending outwards and interacting with the corresponding carbon chains of the surface mycoloyl glycolipids, such as trehalose 6,6′-dimycolate (TDM) and glucose monomycolate (GMM). These packed mycolic acids and mycolic acid-containing glycolipids primarily account for the highly hydrophobic properties of the cell wall of mycobacteria, providing a molecular basis for resistance to treatment with acid alcohol. An anti-tuberculosis drug, isoniazid, exerts its bactericidal effects by specifically inhibiting biosynthesis of mycolic acids, underscoring that mycolic acids (and mycolic acid-containing glycolipids) are essential for survival of mycobacteria [2].

In terms of host defense, it is reasonable to speculate that immune responses directed against such critical lipid components would play an important role in protective immunity. Indeed, recent studies have identified a novel pathway for mycobacterial lipid-specific T cell responses, mediated by human group 1 CD1 molecules (CD1a, CD1b, and CD1c) [3–7]. Upon infection with mycobacteria, these CD1 molecules, expressed in the dendritic cell lineage of professional antigen-presenting cells, capture mycobacteria-derived lipid antigens and present them to

* Corresponding author. Fax: +81 75 752 3232.
E-mail address: msugita@virus.kyoto-u.ac.jp (M. Sugita).

0006-291X/$ - see front matter © 2005 Elsevier Inc. All rights reserved.
doi:10.1016/j.bbrc.2005.09.070

T cells bearing the αβ T cell receptor (TCR). Subsequently, these T cells detect and lyse mycobacteria-infected cells and eliminate live mycobacteria, thereby contributing to clearing mycobacterial infection [8]. Furthermore, potential importance of the lipid-specific T cell response in vivo in host defense against infection with mycobacteria was demonstrated in the guinea pig model of human tuberculosis [9]. Taken together, these observations have highlighted a new aspect of protective immunity against mycobacterial infection that has never been appreciated previously.

In this line of studies, we have particularly directed our attention to GMM-specific T cell responses for the following reasons: (1) only after live infection, GMM is produced in mycobacteria by utilizing host-derived glucose as the carbohydrate source, and thus, GMM-specific T cell responses are directly associated with active infection [5,6]; (2) GMM-specific, CD1b-restricted T cells are mobilized to the mycobacteria-infected skin lesions of a leprosy patient and are shown to function against mycobacterial infection [6,8,10]; (3) the X-ray crystallographic analysis provided a solid molecular evidence for interaction between GMM and human CD1b [11]. However, little is known about environmental factors and stimuli that may affect GMM production by mycobacteria. Given that mycobacteria could potentially undergo thermally adaptive changes in the cell wall lipid composition [12], we addressed the possibility that GMM biosynthesis might be temperature dependent. In the present study, we show that GMM is produced in abundance at reduced temperature and recognized by specific CD1b-restricted T cells. Based on these observations, implications for host defense against mycobacterial infection are discussed.

Materials and methods

Bacterial culture. Mycobacterium smegmatis (ATCC 14468) was grown in Middlebrook 7H9 medium supplemented with ADC enrichment (BD Diagnostic Systems, Sparks, MD). The cultivation was performed with shaking either at 37 or at 30 °C, and bacteria were harvested at their midlog phase growth.

Lipid extraction and thin-layer chromatography. Bacterial culture was centrifuged, and the total lipids were extracted from the pellet with 20 volumes of chloroform/methanol (C/M) (2:1, vol/vol) for 1 h at room temperature. After centrifugation at 1500*g*, the supernatant was collected, and the pellet was reextracted sequentially with C/M (1:1, vol/vol) and C/M (1:2, vol/vol). Finally, all the three pooled supernatants were combined and herein referred to as "total lipids." The total lipids thus obtained were separated by thin-layer chromatography (TLC) on silica gel plates (Analtech, Newark, DE) in a solvent of chloroform/methanol/acetone/acetic acid (90:10:6:1, vol/vol/vol/vol), together with *Mycobacterium phlei*-derived GMM [6] and *Mycobacterium tuberculosis*-derived TDM (Nacalai Tesque, Kyoto, Japan) as reference lipids. Glycolipid spots were visualized with a 9 M sulfuric acid spray followed by charring at 180 °C for analytical purposes or with iodine vapor for preparative purposes.

Purification of GMM. Glycolipid spots were visualized with iodine vapor, and the spot corresponding to GMM was scraped off the silica gel plate, followed by elution in C/M (2:1, vol/vol). GMM was purified by repeating TLC separation until the purified material was represented as a single spot on the TLC plate. The purified samples were then analyzed structurally by matrix-assisted laser desorption ionization-time of flight (MALDI-TOF) mass spectrometry and functionally by T cell stimulation assays using a GMM-specific T cell line as described below.

Mass spectrometry. MALDI-TOF mass spectra were acquired on a Voyager-DE STR mass spectrometer (Applied Biosystems, Foster City, CA) with a pulse laser emitting at 337 nm. Samples were analyzed in the reflectron mode with an accelerating voltage operating in positive ion mode of 20 kV. An external mass spectrum calibration was performed using calibration mixture 2 of the Sequazyme Peptide Mass Standards kit (PerSeptive Biosystems, Framingham, MA), including known peptide standards in a mass range from 1290 to 5700 Da.

T cell stimulation assays. T cell stimulation assays detecting presentation of GMM to specific T cells were carried out as described previously [13]. Briefly, a human B-lymphoblastoid cell line (C1R) stably transfected with either CD1b or vector alone [14] was incubated overnight with 1 μg/ml of the GMM preparation, washed, and fixed with 0.08% glutaraldehyde. Subsequently, the T cell receptor (TCR)-deficient T cell line (J.RT3) reconstituted with the GMM-specific, CD1b-restricted TCR (J.RT3/LDN5) [13] was cultured with these fixed C1R transfectants in the presence of 10 ng/ml phorbol myristate acetate (Sigma–Aldrich, St. Louis, MO). Aliquots of the culture supernatants were collected after 20 h, and the amount of interleukin-2 (IL-2) released into the supernatants was measured, using a commercial enzyme-linked immunosorbent assay kit (BD Biosciences, San Jose, CA).

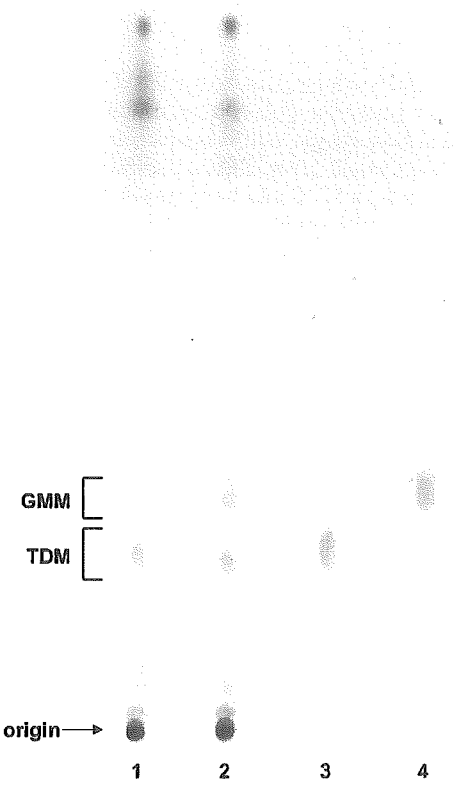

Fig. 1. Analytical TLC, detecting mycoloyl glycolipids. The total lipid fractions were obtained from *M. smegmatis* grown either at 37 °C (lane 1) or at 30 °C (lane 2), and analyzed on a TLC plate along with purified TDM derived from *M. tuberculosis* (lane 3) and GMM derived from *M. phlei* (lane 4) as reference glycolipids. The position of spots representing GMM, TDM, and the origin is indicated to the left of the plate. Note that the TDM species produced by *M. tuberculosis* contain carbon chains longer than those produced by *M. smegmatis*, resulting in a slightly faster migration of the former species.

Results and discussion

Upregulation of GMM biosynthesis in mycobacteria at reduced temperature

Human T cells recognizing mycobacteria-derived GMM in the context of CD1 molecules were detected in mycobacteria-infected tissues, and their significance in host defense against mycobacterial infection has recently been emphasized [5,8]. Thus, the amount of GMM produced in mycobacteria may critically influence the magnitude and quality of the host protective immunity, but little is known about potential stimuli and environmental factors that may upregulate GMM biosynthesis. Previous studies, including ours, have provided evidence that the cell wall mycolic acid species as well as the membrane lipid composition of mycobacteria are influenced by growth temperature [12,15]. Therefore, in the present study, we addressed the possibility that efficiency in GMM biosynthesis might be affected by growth temperature.

Mycobacterium smegmatis was grown in standard 7H9 medium either at 37 or at 30 °C, and the cells were harvested at the midlog phase growth. The rate of cell division and growth was not apparently affected at the reduced temperature. The total lipids were extracted and applied to a silica gel TLC plate, followed by development in chloroform/methanol/acetone/acetic acid (90:10:6:1, vol/vol/vol/vol). We chose this solvent mixture since it allowed us to achieve a fairly good resolution of mycolate-containing glycolipids derived from mycobacteria. Indeed, as shown in Fig. 1, purified GMM (lane 4) was well separated from trehalose 6,6′-dimycolate (TDM) (lane 3) under these conditions. Along with these reference glycolipids, each of the total lipid preparations that were obtained from mycobacteria grown either at 37 or at 30 °C was loaded at an equal quantity (100 μg per lane) and analyzed on the TLC plate. A spot corresponding to TDM was apparent in the total lipid preparation from mycobacteria grown at 37 °C, but a spot corresponding to GMM was hardly visible (lane 1). In contrast, a spot likely to represent GMM was readily detectable in the total lipid preparation from mycobacteria grown at 30 °C (lane 2). Thus, unlike TDM that was synthesized in a similar amount at 37 and at 30 °C, the prominent production of GMM was observed only at the reduced temperature, underscoring its growth temperature-dependent biosynthesis.

MALDI-TOF mass spectrometry analysis of the GMM spot

The identity of the TLC spot as GMM was further confirmed by mass spectrometric analysis. The total lipids derived from mycobacteria grown at 30 °C were resolved on a preparative TLC plate, and lipids recovered from the spot of our focus were subjected to MALDI-TOF mass spectrometry. Natural mycolic acids generally occur as a series of structurally related molecules that differ in the length of carbon chains, the number of double bonds and cyclopropane rings, and the structure of an associated R group [16], and thus, mycolic acid-containing glycolipids, such as GMM, generate complex mass spectra. Indeed, positive MALDI-TOF mass spectra of the possible GMM

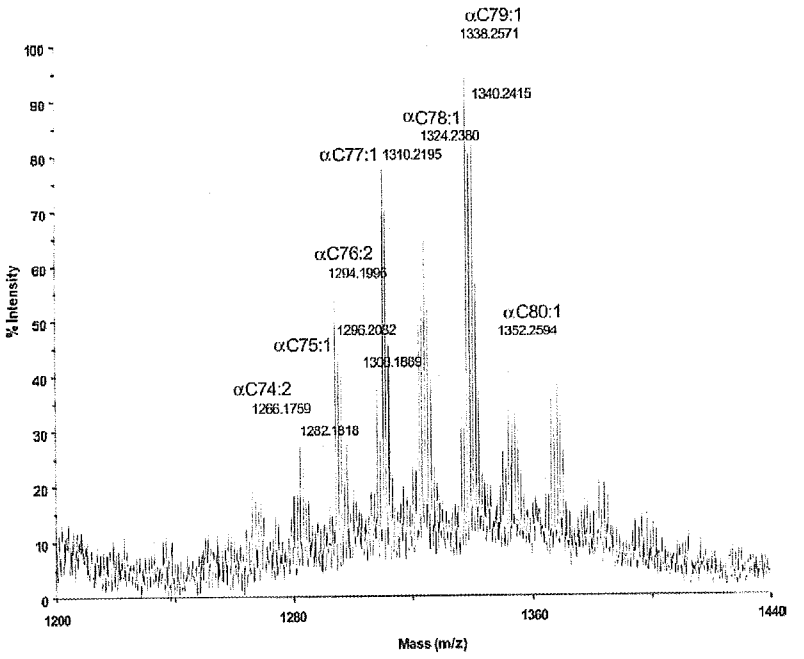

Fig. 2. MALDI-TOF mass spectra of the GMM preparation that was derived from *M. smegmatis* grown at 30 °C. The sample was dissolved in chloroform/methanol (2:1, vol/vol) at a concentration of 1 mg/ml and applied on the sample plate as 0.75 μl droplets. 2,5-DHB was used as matrix. The accelerating voltage was 20 kV (TOF ion-trapping; positive reflectron mode).

spot on TLC showed wide pseudomolecular ion $[M + Na]^+$ distribution ranging from m/z 1266 to m/z 1384, and a majority of peaks accorded with GMM consisting of α-mycolate (C_{74}, C_{76}, C_{77}, C_{78}, C_{79}, or C_{80}) that contained one or two double bonds in the carbon chains with or without a methyl branch (Fig. 2). Combined gas chromatography–mass spectrometry analysis of alditol acetate derivatives obtained from the lipid preparation further confirmed that glucose was the only species of the sugar moiety attached to mycolic acids (data not shown). Taken together, these TLC and mass spectrometric findings established for the first time the growth temperature-dependent nature of GMM biosynthesis in mycobacteria.

CD1-restricted T cell recognition of GMM produced at reduced temperature

Previously, a mycobacteria-specific T cell line (LDN5) was derived from mycobacteria-infected skin lesions of a leprosy patient, and subsequent studies revealed that the LDN5 cells specifically recognized mycobacteria-derived GMM in a CD1b-restricted fashion [6,10]. Further, these T cells efficiently recognized and lysed mycobacteria-infected cells, suggesting that the GMM-specific T cell response could be induced at the site of infection and mediate protective immunity against mycobacterial infection [8].

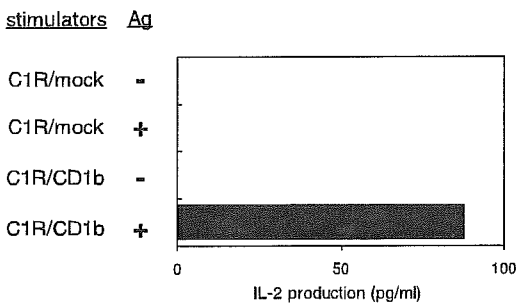

Fig. 3. Stimulation of GMM-specific, CD1b-restricted T cells by the GMM preparation that was derived from *M. smegmatis* grown at 30 °C. The LDN5 TCR-reconstituted J.RT3 cells (J.RT3/LDN5) were tested for their ability to respond to C1R transfectant cells that were pulsed with or without the GMM preparation. The specific T cell response was assessed by measuring IL-2 released into the culture medium.

In order to address whether GMM abundantly expressed at reduced temperature might function as T cell antigen recognized by LDN5 cells, a human B-lymphoblastoid cell line (C1R) that was either mock transfected (C1R/mock) or transfected with CD1b cDNA (C1R/CD1b) was incubated with or without GMM obtained from mycobacteria grown at 30 °C, and used as stimulator cells. As responder T cells, T cell receptor (TCR)-deficient Jurkat cells (J.RT3) reconstituted with the LDN5 TCR by transfection (J.RT3/LDN5) were prepared. As shown in Fig. 3, only C1R/CD1b cells that were pulsed with the antigen preparation specifically stimulated J.RT3/LDN5 cells to secrete interleukin-2 (IL-2), providing a solid evidence that GMM produced at reduced temperature could potentially be recognized by human T cells.

GMM as an indicator for local invasion of mycobacteria

A series of previous works demonstrated that mycobacteria were incapable of synthesizing GMM without supply of glucose, but could potentially acquire exogenous glucose from the culture media or from host tissues and esterify it to mycolic acids to generate GMM [5,6]. Based on the consideration that glucose is not generally found in abundance in mycobacterial growth environments other than in infected host tissues, it has been proposed that immune detection of GMM would be a valuable strategy that the host wisely employs to monitor mycobacterial infection.

However, given that GMM is produced inefficiently at 37 °C but more abundantly at reduced temperature, this

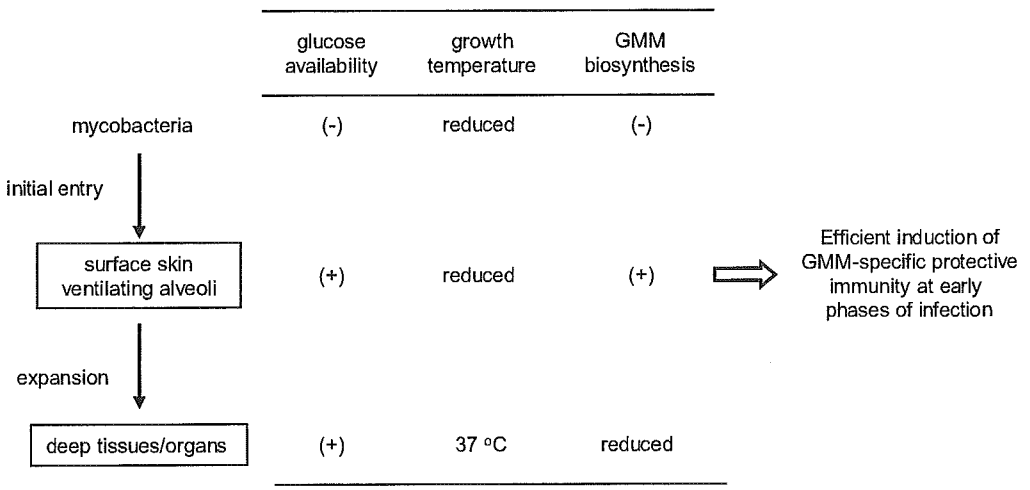

Fig. 4. A proposed model for GMM biosynthesis in mycobacteria at each step of infection. Invading mycobacteria encounter the high glucose and low temperature environments only at the early phases of infection, when accelerating production of GMM occurs in situ. This results in efficient induction of the GMM-specific host defense against mycobacterial infection.

hypothesis may need some modifications by taking both glucose availability and growth temperature into account. As illustrated in Fig. 4, without direct interaction with the host, mycobacteria are incapable of producing GMM due to poor glucose availability, but immediately after infection, the bacteria are exposed to high concentrations of host glucose that are sufficient for GMM biosynthesis [5]. It should also be noted that the common portal sites for mycobacteria to primarily infect include ventilating alveoli of the lung and the externally exposed skin that often render invading microbes survive at reduced temperature [17–19]. Thus, these high glucose and low temperature environments support accelerated production of GMM in mycobacteria, leading to efficient induction of the GMM-specific, CD1-restricted T cell response. In contrast, when mycobacteria expand and invade deeply into tissues and other internal organs, where the temperature is kept constantly around 37 °C, the rate of GMM biosynthesis would be significantly decreased. Thus, GMM would be preferentially produced at the local sites of primary infection and may function as a sensitive indicator for initial invasion into host tissues.

The GMM-specific T cell response is proposed to mediate protective immunity against mycobacterial infection, and an attempt to test GMM as a potential anti-tuberculosis vaccine is currently being made. The observations in the present study and the discussion above emphasize that the GMM vaccine would confer protective immunity that is associated with prevention of initial invasion of mycobacteria into host tissues, and thus, would be ideal for prophylactic applications.

Acknowledgments

We thank Dr. D.B. Moody, Harvard Medical School, for providing purified GMM derived from *Mycobacterium phlei*. This work was supported by grants from the Ministry of Education, Culture, Sports, Science and Technology (Grant-in-Aid from Scientific Research on Priority Areas #16017298 and #17047023), from Japan Society for the Promotion of Science (Grant-in-Aid for Scientific Research (B) #15390317), and from Takeda Science Foundation (to M.S.).

References

[1] P.J. Brennan, Structure, function, and biogenesis of the cell wall of *Mycobacterium tuberculosis*, Tuberculosis (Edinb.) 83 (2003) 91–97.

[2] A. Banerjee, E. Dubnau, A. Quemard, V. Balasubramanian, K.S. Um, T. Wilson, D. Collins, G. de Lisle, W.R. Jacobs Jr., inhA, a gene encoding a target for isoniazid and ethionamide in *Mycobacterium tuberculosis*, Science 263 (1994) 227–230.

[3] E.M. Beckman, S.A. Porcelli, C.T. Morita, S.M. Behar, S.T. Furlong, M.B. Brenner, Recognition of a lipid antigen by CD1-restricted alpha beta+ T cells, Nature 372 (1994) 691–694.

[4] I. Matsunaga, A. Bhatt, D.C. Young, T.Y. Cheng, S.J. Eyles, G.S. Besra, V. Briken, S.A. Porcelli, C.E. Costello, W.R. Jacobs Jr., D.B. Moody, *Mycobacterium tuberculosis* pks12 produces a novel polyketide presented by CD1c to T cells, J. Exp. Med. 200 (2004) 1559–1569.

[5] D.B. Moody, M.R. Guy, E. Grant, T.Y. Cheng, M.B. Brenner, G.S. Besra, S.A. Porcelli, CD1b-mediated T cell recognition of a glycolipid antigen generated from mycobacterial lipid and host carbohydrate during infection, J. Exp. Med. 192 (2000) 965–976.

[6] D.B. Moody, B.B. Reinhold, M.R. Guy, E.M. Beckman, D.E. Frederique, S.T. Furlong, S. Ye, V.N. Reinhold, P.A. Sieling, R.L. Modlin, G.S. Besra, S.A. Porcelli, Structural requirements for glycolipid antigen recognition by CD1b-restricted T cells, Science 278 (1997) 283–286.

[7] J.P. Rosat, E.P. Grant, E.M. Beckman, C.C. Dascher, P.A. Sieling, D. Frederique, R.L. Modlin, S.A. Porcelli, S.T. Furlong, M.B. Brenner, CD1-restricted microbial lipid antigen-specific recognition found in the $CD8^+$ alpha beta T cell pool, J. Immunol. 162 (1999) 366–371.

[8] S. Stenger, R.J. Mazzaccaro, K. Uyemura, S. Cho, P.F. Barnes, J.P. Rosat, A. Sette, M.B. Brenner, S.A. Porcelli, B.R. Bloom, R.L. Modlin, Differential effects of cytolytic T cell subsets on intracellular infection, Science 276 (1997) 1684–1687.

[9] C.C. Dascher, K. Hiromatsu, X. Xiong, C. Morehouse, G. Watts, G. Liu, D.N. McMurray, K.P. LeClair, S.A. Porcelli, M.B. Brenner, Immunization with a mycobacterial lipid vaccine improves pulmonary pathology in the guinea pig model of tuberculosis, Int. Immunol. 15 (2003) 915–925.

[10] P.A. Sieling, D. Chatterjee, S.A. Porcelli, T.I. Prigozy, R.J. Mazzaccaro, T. Soriano, B.R. Bloom, M.B. Brenner, M. Kronenberg, P.J. Brennan, et al., CD1-restricted T cell recognition of microbial lipoglycan antigens, Science 269 (1995) 227–230.

[11] T. Batuwangala, D. Shepherd, S.D. Gadola, K.J. Gibson, N.R. Zaccai, A.R. Fersht, G.S. Besra, V. Cerundolo, E.Y. Jones, The crystal structure of human CD1b with a bound bacterial glycolipid, J. Immunol. 172 (2004) 2382–2388.

[12] T. Baba, K. Kaneda, E. Kusunose, M. Kusunose, I. Yano, Thermally adaptive changes of mycolic acids in *Mycobacterium smegmatis*, J. Biochem. (Tokyo) 106 (1989) 81–86.

[13] M. Sugita, E.P. Grant, E. van Donselaar, V.W. Hsu, R.A. Rogers, P.J. Peters, M.B. Brenner, Separate pathways for antigen presentation by CD1 molecules, Immunity 11 (1999) 743–752.

[14] M. Sugita, S.A. Porcelli, M.B. Brenner, Assembly and retention of CD1b heavy chains in the endoplasmic reticulum, J. Immunol. 159 (1997) 2358–2365.

[15] M. Suutari, S. Laakso, Effect of growth temperature on the fatty acid composition of *Mycobacterium phlei*, Arch. Microbiol. 159 (1993) 119–123.

[16] Y. Fujita, T. Naka, T. Doi, I. Yano, Direct molecular mass determination of trehalose monomycolate from 11 species of mycobacteria by MALDI-TOF mass spectrometry, Microbiology 151 (2005) 1443–1452.

[17] N.C. Abbot, J.S. Beck, F. Feval, F. Weiss, M.H. Mobayen, K. Ghazi-Saidi, Y. Dowlati, A.A. Velayati, J.L. Stanford, Immunotherapy with Mycobacterium vaccae and peripheral blood flow in long-treated leprosy patients, a randomised, placebo-controlled trial, Eur. J. Vasc. Endovasc. Surg. 24 (2002) 202–208.

[18] N.C. Abbot, J.S. Beck, P.D. Samson, C.R. Butlin, P.J. Bennett, J.M. Grange, Cold fingers in leprosy, Int. J. Lepr. Other Mycobact. Dis. 60 (1992) 580–586.

[19] N.S. Pilipchuk, I.V. Prokhorovich, V.I. Petrenko, [The results of pneumothermometry and mucociliary clearance study in pulmonary tuberculosis patients], Vrach. Delo (1991) 49–53.

BRIEF REPORT

Identification of Attenuated Variants of HIV-1 Circulating Recombinant Form 01_AE That Are Associated with Slow Disease Progression Due to Gross Genetic Alterations in the *nef*/Long Terminal Repeat Sequences

Makiko Kondo,[1] Takako Shima,[1] Masako Nishizawa,[3] Koji Sudo,[1] Shinya Iwamuro,[2] Takeshi Okabe,[2] Yutaka Takebe,[4] and Mitsunobu Imai[1]

[1]Division of Microbiology, Kanagawa Prefectural Institute of Public Health, and [2]Atsugi City Hospital, Kanagawa, and [3]AIDS Research Center, National Institute of Infectious Diseases, Musashimurayama, and [4]AIDS Research Center, National Institute of Infectious Diseases, Shinjuku-ku, Tokyo, Japan

We identified an unusual case of human immunodeficiency virus type 1 (HIV-1) infection in a patient (GM43) who exhibited a persistently low antibody response and undetectable viral load during a 5-year follow-up period. GM43 harbored HIV-1 circulating recombinant form 01_AE with gross deletions in the *nef*/long terminal repeat (LTR) region. The sizes of the deletions increased progressively from 84 to >400 bp during the 5-year period. GM43 appeared to have acquired defective variants from her husband. The genetic alterations in the *nef*/LTR region were remarkably similar to those that have been reported in slow progressors (such as the slow progressors in the Sydney Blood Bank Cohort). The present study is the first report of slow disease progression due to gross genetic alterations in the *nef*/LTR region in a person infected with an HIV-1 non–subtype B strain.

Rates of disease progression vary among individuals infected with HIV-1, because of the complex interplay between host genetic and immunologic factors and the pathogenic potential of the infecting virus. The viral *nef* gene is one of the crucial determinants of disease progression, as has been demonstrated in animal models [1–3]. That the *nef* gene is a key factor for disease progression in humans is strongly supported by the finding that some long-term nonprogressors (LTNPs) with low viral loads (despite 10–14 years of HIV-1 infection) carry viruses with gross deletions [4–6] or small structural defects and mutations [7] in the *nef* gene.

The *nef* gene is known to have pleiotropic functions, including down-regulation of the cell-surface expression of CD4 and class I major histocompatibility complex (MHC) molecules, enhancement of viral replication and infectivity, induction of cytokine and chemokine expression by T cells and macrophages, and blockage of proapoptotic signaling by HIV-1–infected cells (reviewed in Geyer et al. [8]). A large number of cellular interaction partners critical to *nef* gene functions have been identified, and the binding sites have been mapped to distinct locations within the Nef protein (reviewed in Geyer et al. [8]).

Although the genetic alterations in the *nef* gene that are associated with slow disease progression have been identified in HIV-1 subtype B in US and European populations [4–7], it remains unclear whether these alterations are found only in the subtype B lineage. In the present study, we identified attenuated variants of HIV-1 circulating recombinant form 01_AE (CRF01_AE) that harbored gross deletions in the *nef*/long terminal repeat (LTR) region in an asymptomatic patient (GM43) who had an unusually weak antibody response and an undetectable viral load during a 5-year follow-up period, demonstrating the association between *nef*/LTR deletions and slow disease progression with respect to infection with a non–subtype B strain.

Patients, materials, and methods. Informed consent was obtained from the patients, and the study was conducted in accordance with the clinical research guidelines of Japan. Antibodies to HIV-1 were detected by use of the Serodia HIV-1 gelatin particle agglutination (PA) test (Fujirebio), and Western-blot (WB) analysis (LAV Blot I; Bio-Rad) was used for confirmation. Plasma HIV-1 RNA loads were measured by the ultrasensitive method with the Amplicor HIV-1 Monitor Kit (version 1.5; Roche Diagnostics), which allows the sensitive

Received 7 September 2004; accepted 9 February 2005; electronically published 25 May 2005.

Reprints or correspondence: Dr. Mitsunobu Imai, Div. of Microbiology, Kanagawa Prefectural Institute of Public Health, 1-3-1 Shimomachiya, Chigasaki-shi, Kanagawa 253-0087, Japan (imaim@d2.dion.ne.jp); or, Dr. Yutaka Takebe, Laboratory of Molecular Virology and Epidemiology, AIDS Research Center, National Institute of Infectious Diseases, Toyama 1-23-1, Shinjuku-ku, Tokyo 162-8640, Japan (takebe@nih.go.jp).

The Journal of Infectious Diseases 2005;192:56–61

0022-1899/2005/19201-0010$15.00

Presented in part: XIV International AIDS Conference, Barcelona, Spain, 10 July 2002 (abstract WePeC6234).

Financial support: Grants from AIDS study groups sponsored by the Ministry of Health, Labor, and Welfare, Japan; Japanese Foundation for AIDS Prevention Research Resident Program (to K.S.).

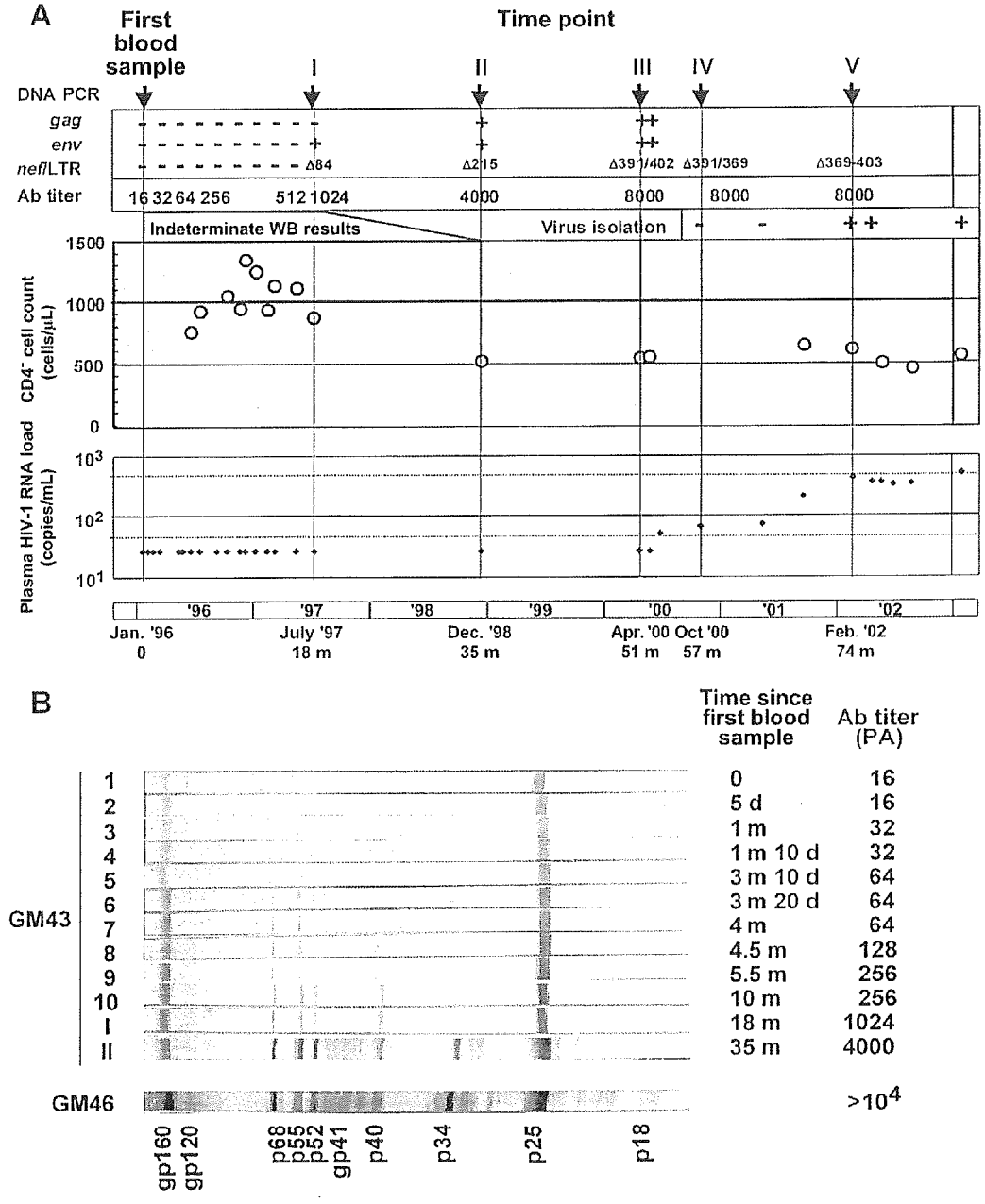

Figure 1. Changes in serological and virological parameters in patient GM43. *A,* Profiles of serological and virological parameters. *Top,* Detection of proviral HIV-1 DNA by nested polymerase chain reaction (PCR) for *gag* (p24), *env* (C2/V3), and the *nef*/long terminal repeat (LTR) region. Antibody (Ab) titers (determined by the Serodia HIV-1 gelatin particle agglutination [PA] test) are also shown. −, negative; +, positive; Δ, the size (in base pairs) of the deletion in the *nef*/LTR region in major PCR products; WB, Western blot. *Middle,* $CD4^+$ cell count, in cells per microliter of blood *(white circles). Bottom,* Plasma HIV-1 RNA load, in copies per milliliter of blood (log scale) *(black diamonds).* HIV-1 proviral genomes were analyzed by use of the serum samples collected at the indicated time points (I–V). HIV-1 was isolated from GM43 for the first time in February 2002 (time point V). *B,* WB analysis (LAV Blot I; Bio-Rad) for GM43 and her husband, GM46. Strips 1–10 are for serum samples serially collected between January and October 1996, and strips I and II are for serum samples collected in July 1997 (time point I) and December 1998 (time point II). d, day; m, month.

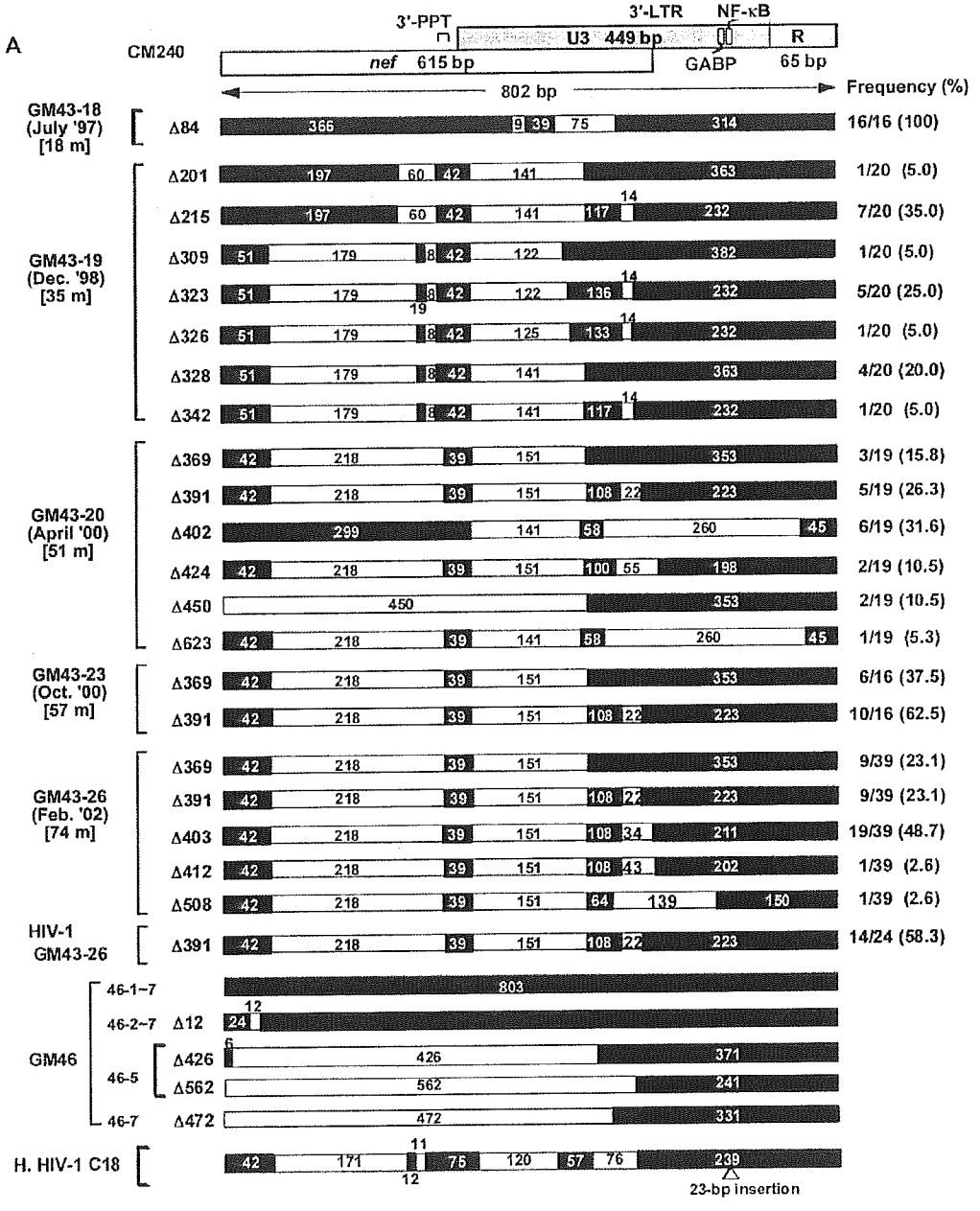

Figure 2. Genomic organization of the *nef*/long terminal repeat (LTR) region. *A*, Schematic drawing of the genomic structure of HIV-1 circulating recombinant form (CRF) 01_AE CM240 [12] for the corresponding region, at top. The genomic organizations of HIV-1 isolates from patient GM43 and her husband, GM46, and of HIV-1 variant C18 (an attenuated variant of HIV-1 subtype B detected in the Sydney Blood Bank Cohort [5]) are shown for comparison. Black bars represent amplified sequences, and white bars represent deletions. The nucleotide positions are shown relative to CM240. The numbers in the white bars represent the sizes of the deletions. m, month; PPT, polypurine tract. *B*, Comparison of the genetic organization of the *nef*/LTR region in GM43-20, a major quasispecies (Δ391) found in GM43, with that of C18 [5]. *C*, Sequence landmarks and the sites of deletions in the *nef*/LTR region in GM43-20. C18 carries a 23-bp duplication comprised of a single set of NF-κB and Sp1 sequences.

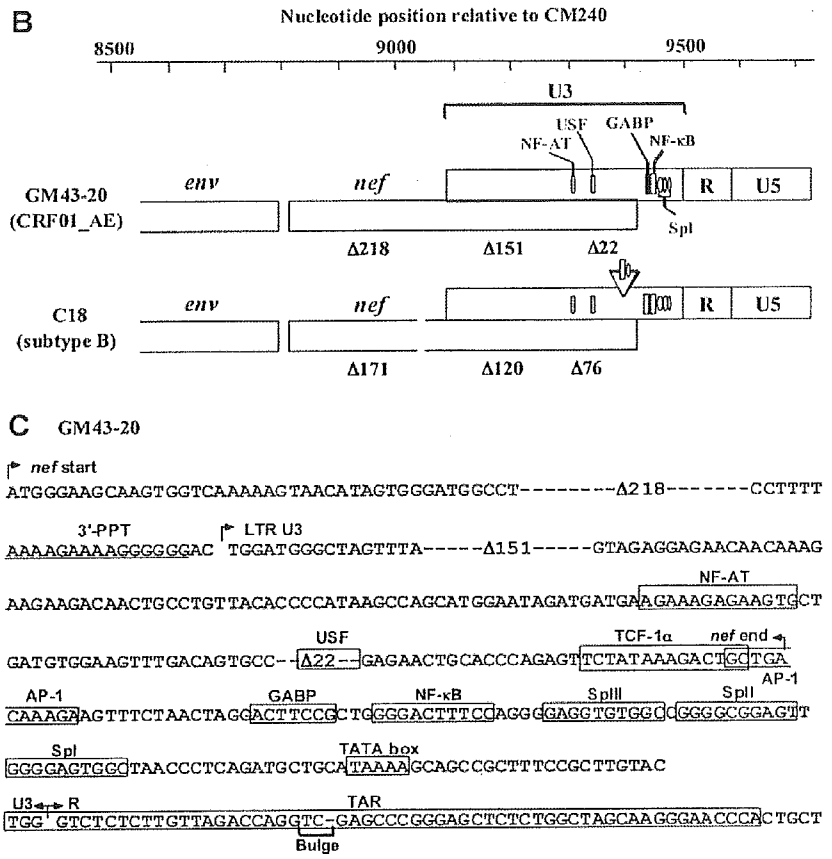

Figure 2. *(Continued.)*

detection of HIV-l RNA from both HIV-1 subtype B and non–subtype B strains, including CRF01_AE [9]. Replication-competent HIV-1 strains were isolated by cocultivation with CD8-depleted peripheral-blood mononuclear cells (PBMCs) from healthy donors. PBMCs were activated by use of anti-CD3 antibody (CLB-CD3; PeliCluster), instead of the standard activation stimuli of phytohemagglutinin and interleukin-2, to improve the efficiency of isolation [10, 11].

The *nef*/LTR regions of HIV-1 provirus genomes were amplified by nested polymerase chain reaction (PCR), with the outer primers Env43F14 (sense; 5′-GAGTTAGGCAGGGATACTCAC-3′; positions 7892–7912 of the genome of CM240, the HIV-1 CRF01_AE reference strain [12]) and 3′LTR43R16 (antisense; 5′-TAAGCACTCAAGGCAAGC-3′; positions 9202–9185 of the genome of CM240) and the inner primers Env43F15 (sense; 5′-AGCCTGTGCCTCTTCAGCTACCA-3′; positions 8052–8083 of the genome of CM240) and MSR5 (antisense; 5′-GCACTCAAGGCAAGCTTTATTGAGGCT-3′; positions 9199–9173 of the genome of CM240). The nucleotide sequences of both strands were determined by the BigDye Terminator cycle sequencing method, using a Prism 310 DNA Sequencer (Applied Biosystems). Nucleotide sequences (GenBank accession numbers AB193797–AB193800) were aligned by use of CLUSTAL W (version 1.4). Phylogenetic trees were constructed by the neighbor-joining method, based on Kimura's 2-parameter distance matrix with 100 bootstrap replicates. Analyses were implemented by use of PHYLIP (version 3.573) [13].

Results. GM43 is a 28-year-old Thai woman who has lived in Japan for the past 6 years. GM43 was infected with HIV-1 via her husband, GM46. GM46 had contracted HIV-1 via heterosexual contact before 1995, presumably in Thailand. Both GM43 and GM46 remain healthy and do not have any clinical symptoms. There is no indication of HIV-2 infection. In January 1996, serologic tests conducted for GM43 at her 18th week of pregnancy (her first visit) showed low marginal HIV-1 seropositivity, with a PA antibody titer of 1:16 (figure 1*A*). Indeterminate WB results (1+ reactivity for gp160 only) persisted for GM43 throughout an 18-month observation period, whereas GM46 was unequivocally positive by WB (figure 1*B*). Empirically, in most HIV-1–infected patients, PA antibody titers

exceed $1:10^3$ within 2 weeks of seroconversion and reach $1:10^4$ one month after seroconversion. However, in GM43, low PA antibody titers ($<1:10^3$) persisted for 1.5 years, and it took >4.5 years until her PA antibody titer reached $1:10^4$ (figure 1*A*).

In parallel with this slow process of seroconversion, GM43's plasma HIV-1 RNA load was persistently below the limit of detection by PCR (<50 copies/mL) during a 4.5-year period (figure 1*A*). HIV-1 proviral DNAs were amplified by nested PCR for the *env* (C2/V3) region only in July 1997 and for both the *gag* (p17) and *env* (C2/V3) regions in December 1998 (figure 1*A*), providing conclusive evidence that GM43 was infected with HIV-1. During the first 3 years after seroconversion, GM43's $CD4^+$ cell count gradually decreased, from 1074 to 600 cells/μL, as her plasma HIV-1 RNA load gradually increased, but her $CD4^+$ cell count remained stable thereafter, at 400–600 cells/μL (figure 1*A*).

To investigate the mechanism of this unusual clinical course, we examined the structural features of the *nef*/LTR region that are known to be associated with slow disease progression [4–6]. The *nef*/LTR regions of HIV-1 proviral genomes were amplified by nested PCR from the PBMC DNAs sampled at 5 different time points between July 1997 and February 2002 (time points I–V, as shown in figure 1). Although the expected size of amplicons of the *nef*/LTR region of the intact HIV-1 genome is 1140 bp, the resulting amplified fragments ranged in size from 500 to 1000 bp, indicating the existence of deletions of ~100–500 bp in the *nef*/LTR region.

To further characterize the genetic alterations in the *nef*/LTR region for GM43, we molecularly cloned (by the TA cloning method) the PCR products and determined the nucleotide sequences of 16–39 independent PCR clones at each time point. Nucleotide-sequence alignment revealed progressive deletions in the *nef*/LTR region over time (figure 2). Plasma HIV-1 RNA load was detectable after the increased deletions in the *nef*/LTR region (time points III–V). A replication-competent HIV-1 strain (GM43-23) was isolated for the first time at time point V. The HIV-1 quasispecies with the 391-bp *nef*/LTR deletion (Δ391) appeared to constitute a major functional (replication-competent) segment of the proviral population in GM43.

We next analyzed the structural characteristics of the HIV-1 genomes for GM46. We attempted to amplify the *nef*/LTR region by PCR at 7 time points (time points 46-1 through 46-7, as shown in figure 2*A*) between 1996 and 1997 (GM46 then dropped out of the follow-up). At all sampling points except the first (46-1), both full-sized and smaller-sized PCR products (containing deletions ranging in size from 12 to 472 bp) were amplified (figure 2*A*) in independent PCR amplification experiments. Although we were not able to establish the exact frequency of defective genomes in GM46, considerable proportions of the HIV-1 quasispecies in GM46 appeared to contain gross genetic alterations in the *nef*/LTR region, especially at later time points. In contrast, no appreciable defects in the *nef*/LTR region were detected among 73 other CRF01_AE–infected individuals (of both Japanese and Thai nationality) in Japan. Phylogenetic-tree analysis based on nucleotide sequences of *env* (C2/V3) and the *nef*/LTR region revealed that HIV-1 sequences from GM43 and GM46 formed a monophyletic cluster within CRF01_AE, with high bootstrap support (100% and 98%, respectively) (data not shown). Furthermore, this GM43/GM46 cluster was distinct from other CRF01_AE local control sequences sampled in the same geographical region. These findings strongly suggest that GM43 was indeed infected via her husband. However, none of the deletions detected in GM46 were identical to those detected in GM43 (figure 2).

The genetic organization of *nef*/LTR deletions detected in GM43 and GM46 are summarized in figure 2. Two large deletions were detected. The first large deletion was located in the amino-terminal half of the *nef* gene that does not overlap with the LTR sequences. The second large deletion was mapped to the *nef*/U3–overlapping region. One or 2 small, additional deletions followed the 2 large deletions. Most of the first large deletion removed the highly conserved acidic (EEEE) domain and $(Pxx)_4$ motif, which are essential for Nef function. However, the downstream deletions located in the *nef*/U3 region left intact the polypurine tract (3′-PPT), NF-κB, and SpI binding sites and the TATA box (figure 2), which are indispensable for HIV-1 replication, as was reported in the previous studies of defective subtype B variants in US and European populations [4–6].

The overall structural configuration of the *nef*/LTR deletions found in the CRF01_AE variant infecting GM43 was remarkably similar to that of the attenuated HIV-1 variant C18 (which belongs to HIV-1 subtype B) detected in the Sydney Blood Bank Cohort [5] (figure 2*A* and 2*B*). Of note, the sequence features unique to CRF01_AE—including the GABP motif (5′-ACTTCCG-3′), a single NF-κB [14], an unusual TATA box (5′-TAAAA-3′), and a 2-nt bulge in TAR stems (figure 2)—were detected in GM43. No appreciable direct repeats that may have caused the deletion in the *nef*/LTR region [6] were detected in GM43.

Discussion. We have identified a unique case of CRF01_AE infection, in which a patient, GM43, experienced an unusually slow increase in HIV-1 antibody titers and had an undetectable viral load over a prolonged period of time. GM43 carried attenuated viral variants with a range of *nef*/LTR deletions that were similar to those found in LTNPs infected with HIV-1 subtype B [4–6]. The present study is the first report demonstrating the association between gross *nef*/LTR deletions and slow disease progression in a patient infected with a non–subtype B strain.

As can be seen in figure 2, striking similarities in the alteration of the *nef*/LTR region between subtype B and CRF01_AE were observed. The genetic alterations observed in the *nef*/LTR region of an attenuated subtype B variant detected in the Sydney

Blood Bank Cohort (isolate C18 [5]) and the CRF01_AE variants found in GM43 in the present study removed most of the sequence elements essential for Nef functions—including the highly conserved acidic (EEEE) domain that is required for the down-regulation of class I MHC molecules and the $(Pxx)_4$ motif mediating the interaction between Nef and signaling molecules—and placed downstream sequences out of frame (figure 2). Although a number of deletions were present in the *nef* region that overlapped U3 in the LTR region, none of these alterations affected *cis*-acting elements known to be critical for viral replication, including the 3′-PPT, the U3 terminal sequences, the TATA box, and the NF-κB and SpI binding sites. This convergent manner of evolution of such genetic alterations in the *nef*/LTR sequences implies the presence of the strong selection pressures that maintain the replication capacities in defective HIV-1 genomes.

Phylogenetic-tree analysis demonstrated that GM43 acquired CRF01_AE from her husband, GM46. Interestingly, GM46 was also found to harbor unique sets of *nef*/LTR deletions, although the profiles of the deletions detected in GM46 were not identical to those detected in GM43 (figure 2). It is tempting to speculate that the defective genomes detected in GM43 may have evolved from a minor viral quasispecies carried by GM46 that was not detected in the present study or that was present only transiently at the time of transmission to GM43. If this is the case, the lack of selection for functional *nef* alleles in GM43 during transmission and/or establishment of infection from GM46 is rather surprising, because functional forms of *nef* alleles are quickly and efficiently selected for in rhesus monkeys infected experimentally with *nef*-defective simian immunodeficiency virus [1]. This suggests that, in certain patients, attenuated viral variants might have a selective advantage over HIV-1 strains with an intact *nef* allele. For instance, an efficient immune response may contribute to the selection of *nef*-defective viruses that could escape the cytotoxic T lymphocyte recognition that is critical to the effective control of viral replication [15]. In light of the identification of this unique case of CRF01_AE infection, a systematic search for the viral and host factors that influence disease progression may be warranted—especially in less-studied regions of the HIV-1 epidemic, such as in developing countries in Asia—with a slow increase in antibody titer used as a convenient marker.

Acknowledgments

We thank the staffs of the participating clinics for their help and Dr. Shingo Kato for his valuable advice on virus isolation.

References

1. Kestler HW 3rd, Ringler DJ, Mori K, et al. Importance of the nef gene for maintenance of high virus loads and for development of AIDS. Cell **1991**; 65:651–62.
2. Du Z, Lang SM, Sasseville VG, et al. Identification of a nef allele that causes lymphocyte activation and acute disease in macaque monkeys. Cell **1995**; 82:665–74.
3. Hanna Z, Kay DG, Rebai N, Guimond A, Jothy S, Jolicoeur P. Nef harbors a major determinant of pathogenicity for an AIDS-like disease induced by HIV-1 in transgenic mice. Cell **1998**; 95:163–75.
4. Kirchhoff F, Greenough TC, Brettler DB, Sullivan JL, Desrosiers RC. Absence of intact nef sequences in a long-term survivor with nonprogressive HIV-1 infection [see comments]. N Engl J Med **1995**; 332:228–32.
5. Deacon NJ, Tsykin A, Solomon A, et al. Genomic structure of an attenuated quasi species of HIV-1 from a blood transfusion donor and recipients [see comments]. Science **1995**; 270:988–91.
6. Salvi R, Garbuglia AR, Di Caro A, Pulciani S, Montella F, Benedetto A. Grossly defective nef gene sequences in a human immunodeficiency virus type 1-seropositive long-term nonprogressor. J Virol **1998**; 72:3646–57.
7. Casartelli N, Di Matteo G, Argentini C, et al. Structural defects and variations in the HIV-1 nef gene from rapid, slow and non-progressor children. AIDS **2003**; 17:1291–301.
8. Geyer M, Fackler OT, Peterlin BM. Structure-function relationships in HIV-1 Nef. EMBO Rep **2001**; 2:580–5.
9. Triques K, Coste J, Perret JL, et al. Efficiencies of four versions of the AMPLICOR HIV-1 MONITOR test for quantification of different subtypes of human immunodeficiency virus type 1. J Clin Microbiol **1999**; 37:110–6.
10. Spina CA, Prince HE, Richman DD. Preferential replication of HIV-1 in the CD45RO memory cell subset of primary CD4 lymphocytes in vitro. J Clin Invest **1997**; 99:1774–85.
11. Wong JK, Hezareh M, Gunthard HF, et al. Recovery of replication-competent HIV despite prolonged suppression of plasma viremia. Science **1997**; 278:1291–5.
12. Carr JK, Salminen MO, Koch C, et al. Full-length sequence and mosaic structure of a human immunodeficiency virus type 1 isolate from Thailand. J Virol **1996**; 70:5935–43.
13. Felsenstein J. PHYLIP (phylogeny inference package) version 3.5c. Seattle, WA: Department of Genetics, University of Washington, **1993**.
14. Verhoef K, Sanders RW, Fontaine V, Kitajima S, Berkhout B. Evolution of the human immunodeficiency virus type 1 long terminal repeat promoter by conversion of an NF-kappaB enhancer element into a GABP binding site. J Virol **1999**; 73:1331–40.
15. Mariani R, Kirchhoff F, Greenough TC, Sullivan JL, Desrosiers RC, Skowronski J. High frequency of defective nef alleles in a long-term survivor with nonprogressive human immunodeficiency virus type 1 infection. J Virol **1996**; 70:7752–64.

JOURNAL OF VIROLOGY, Aug. 2005, p. 10386–10396
0022-538X/05/$08.00+0 doi:10.1128/JVI.79.16.10386–10396.2005

Vol. 79, No. 16

Influence of Glycosylation on the Efficacy of an Env-Based Vaccine against Simian Immunodeficiency Virus SIVmac239 in a Macaque AIDS Model

Kazuyasu Mori,[1,2,3]* Chie Sugimoto,[1,2,3] Shinji Ohgimoto,[4] Emi E. Nakayama,[5] Tatsuo Shioda,[5] Shigeru Kusagawa,[1] Yutaka Takebe,[1] Munehide Kano,[1] Tetsuro Matano,[6] Takae Yuasa,[7] Daisuke Kitaguchi,[7] Masaaki Miyazawa,[7] Yumiko Takahashi,[8] Michio Yasunami,[8] Akinori Kimura,[8] Naoki Yamamoto,[1] Yasuo Suzuki,[3,9] and Yoshiyuki Nagai[10]

AIDS Research Center, National Institute of Infectious Diseases, Shinjuku-ku, Tokyo 162-8640,[1] Tsukuba Primate Research Center, National Institute of Biomedical Innovation, Tsukuba, Ibaraki 305-0843,[2] CREST, Japan Science and Technology Agency, Kawaguchi, Saitama 332-0012,[3] Microbiology and Genomics, Department of Genome Sciences, Kobe University School of Medicine, Kobe, Hyogo 650-0017,[4] Department of Viral Infections, Research Institute for Microbial Diseases, Osaka University, Suita, Osaka 565-0871,[5] Department of Microbiology, Graduate School of Medicine, The University of Tokyo, Bunkyo-ku, Tokyo 113-0033,[6] Department of Immunology, Kinki University School of Medicine, Osaka-Sayama, Osaka 589-8511,[7] Department of Molecular Pathogenesis, Division of Medical Science, Medical Research Institute, Tokyo Medical and Dental University, Chiyoda-ku, Tokyo 101-0062,[8] Department of Biochemistry, University of Shizuoka School of Pharmaceutical Sciences and COE Program in the 21st Century, Shizuoka, Shizuoka 422-8526,[9] and Toyama Institute of Health, Kosugi, Toyama 939-0363,[10] Japan

Received 8 December 2004/Accepted 2 May 2005

The envelope glycoprotein (Env) of human immunodeficiency viruses (HIVs) and simian immunodeficiency viruses (SIVs) is heavily glycosylated, and this feature has been speculated to be a reason for the insufficient immune control of these viruses by their hosts. In a macaque AIDS model, we demonstrated that quintuple deglycosylation in Env altered a pathogenic virus, SIVmac239, into a novel attenuated mutant virus (Δ5G). In Δ5G-infected animals, strong protective immunity against SIVmac239 was elicited. These HIV and SIV studies suggested that an understanding of the role of glycosylation is critical in defining not only the virological properties but also the immunogenicity of Env, suggesting that glycosylation in Env could be modified for the development of effective vaccines. To examine the effect of deglycosylation, we constructed prime-boost vaccines consisting of Env from SIVmac239 and Δ5G and compared their immunogenicities and vaccine efficacies by challenge infection with SIVmac239. Vaccination-induced immune responses differed between the two vaccine groups. Both Env-specific cellular and humoral responses were higher in wild-type (wt)-Env-immunized animals than in Δ5G Env-immunized animals. Following the challenge, viral loads in SIVmac239 Env (wt-Env)-immunized animals were significantly lower than in vector controls, with controlled viral replication in the chronic phase. Unexpectedly, viral loads in Δ5G Env-immunized animals were indistinguishable from those in vector controls. This study demonstrated that the prime-boost Env vaccine was effective against homologous SIVmac239 challenge. Changes in glycosylation affected both cell-mediated and humoral immune responses and vaccine efficacy.

Primate lentiviruses, human immunodeficiency viruses (HIVs), and simian immunodeficiency viruses (SIVs) share common genetic and biological properties. As SIVmac, originally isolated from macaques in primate research centers in the United States, causes AIDS in macaques with remarkable similarities to HIV type 1 (HIV-1) infection in humans, this AIDS monkey model has been utilized to study vaccine development and the pathogenesis of HIV infection (for reviews, see references 10, 14, 17, 43, and 47).

HIV/SIV infection in the host consists of two phases, the primary infection and chronic infection. During the primary infection, extensive viral replication and dissemination of the infection occur. In chronic infection, viral replication continues for a long period, eventually leading to AIDS. Due to the host immune response against the infection, these two phases are separated by a set point at which the viral load reaches its lowest level. The viral loads of the set point and chronic infection are inversely correlated with the control of SIV/HIV infection and predict disease progression (25, 31); however, it remains unclear which host responses determine the viral loads of the set point and chronic infection. Nevertheless, virus-specific immune responses have been implicated in the host's control of the infection. Cellular immunity, such as that shown by cytotoxic T lymphocytes (CTL) and helper T cells, has been reported to correlate with the control of HIV/SIV infection (for reviews, see references 2, 24, 28, and 39). The role of the neutralizing antibody (NAb) in the control of infection and the

* Corresponding author. Mailing address: Tsukuba Primate Research Center, National Institute of Biomedical Innovation, 1 Hachimandai, Tsukuba, Ibaraki 305-0843, Japan. Phone: 81-29-837-2121. Fax: 81-29-837-0218. E-mail: mori@nibio.go.jp.

emergence of escape mutants has also been reported previously (7, 16, 51).

Despite these immune responses against HIV/SIV infection, humans and macaques fail to contain the infection due to the virus properties. HIV/SIV infects major target cells, such as $CD4^+$ T cells and macrophages, by binding viral envelope glycoproteins (Env) to cellular surface proteins and CD4 and chemokine receptors (CCR5, CXCR4, or others) on target cells (5, 32). Since viral entry consists of multiple steps (virion binding to these viral receptors, conformational change of Env, and fusion between the virion and the cellular membrane) and the critical parts of Env used in these steps are exposed only during each step, naturally generated antibodies are only partly effective in preventing HIV/SIV infection in their hosts (7, 8). Primary isolates can be neutralized to various degrees by HIV-infected patient serum but not by contemporaneous autologous samples. Consequently, escape mutants against preexisting NAb are selectively replicated (51). Thus, effective NAb is rarely induced in HIV/SIV infection (8, 10). This could partly explain the failure of Env-based vaccine trials against HIV-1 (8, 50).

The heavy glycosylation of Env is a unique feature of HIV/SIV that is distinctive from features of other enveloped viruses and is significantly related to their neutralization-resistant property (8, 29, 44). We therefore assumed that the insufficient immune containment of HIV/SIV might be due to heavy glycosylation in Env and that the removal of some glycans might allow the host to mount a protective immune response against the infection. Thus, we studied the influence of deglycosylation on the replication of SIVmac239 in a T-cell line and created a quintuple deglycosylation mutant of SIVmac239 (Δ5G), which has maximal removal of N-glycans at amino acid residues 79, 146, 171, 460, and 479 in Env and retains a replication capability similar to that of SIVmac239 in phytohemagglutinin-stimulated rhesus peripheral blood mononuclear cells (PBMCs) (36, 40). We then examined the infection of rhesus macaques with Δ5G; although Δ5G was replicated as extensively as SIVmac239 during the primary infection, the subsequent Δ5G infection was restricted to a level less than the detection sensitivity of a plasma viral load assay by 8 weeks postinfection (p.i.), in contrast to high chronic viral replication in SIVmac239 infection. Furthermore, an almost sterilizing immunity against SIVmac239 was induced in Δ5G-infected animals (36). Interestingly, another quintuple-deglycosylation-mutation strain with mutations at amino acid residues 146, 156, 184, 244, and 247 in Env was created (44) and was demonstrated to share common features with Δ5G in viral replication in animals and in functions as an attenuated vaccine (20). Since these two viruses share only one deglycosylation mutation and other mutations distributed differently in surface envelope protein gp120 (SU), these two studies suggest that heavily glycosylated Env determines the pathogenicity of HIV/SIV.

To dissect the mechanism for notable containment of Δ5G infection after primary infection, we hypothesized that the Env of Δ5G, a viral protein that differs from that in SIVmac239, might elicit protective immunity against SIVmac239, because deglycosylation in Env might alter antigenic properties such as B-cell and T-cell epitopes and enhance the protective immunity against SIVmac239. For this purpose, we immunized animals with Env of Δ5G (Δ5G Env) or Env of SIVmac239 (the wild type; wt Env), and examined the effect of these vaccinations against SIVmac239 infection.

MATERIALS AND METHODS

Generation of SU DNA vaccines. DNA vaccine plasmids expressing SIV mac239 SU or Δ5G SU, pJWSUmac239 and pJWSUmacΔ5G, were constructed using the expression vector pJW4303 (45). To produce secreted SU efficiently, the native signal sequence in the SIVmac239 SU gene was replaced with the human tissue plasminogen activator signal in plasmid pJW4303, and a termination codon was created at the cleavage site for SU transmembrane (TM) protein (9). An SIVmac239 SU or Δ5G SU DNA sequence was amplified with a pair of primers, SUmacA (5′-TGTGCTAGCTATGTCACAGTCTTTTATGGTGTAC-3′) and SUmacB (5′-CCAGGATCCTATTACCTCTTCACATCTGTGGGGG C-3′). The SUmacA primer consisted of nucleotides (nt) 6923 to 6955 of the SIVmac239 sequence (GenBank accession number M33262) and the boldface nucleotides, which were changed to create a NheI site; primer SUmacB consisted of nt 8412 to 8381 and the boldface nucleotides, which were changed to create a BamHI site, and the underlined nucleotides, which generated tandem termination codons. The PCR-amplified fragments were digested with NheI and BamHI and cloned into the NheI- and BamHI-digested eukaryotic expression vector pJW4303 to yield pJWSUmac239 and pJWSUmacΔ5G. These plasmids were prepared using a Plasmid Mega kit (QIAGEN, Tokyo, Japan).

Generation of Env vaccinia vaccines. Recombinant vaccinia viruses expressing Env of SIVmac239 or Δ5G, WRvvmac239 or WRvvΔ5G, respectively, were constructed using a vaccinia virus WR strain (WRvv) as described previously (15). To excise the entire coding region of the *env* gene from the cloned SIV plasmid, BamHI and SmaI sites were introduced by in vitro mutagenesis at 5′- and 3′-end-flanking sites of the *env* gene, respectively. Primer B-6808 (5′-GAA AGAGAAGAAGGATCCCGAAAAAGG-3′) consisted of nt 6796 to 9822 and the underlined mutations of the BamHI site; S-9537 (5′-TATGAATACTCCC GGGAGAAACCC-3′) consisted of nt 9527 to 9550 and the underlined mutations of the SmaI site. DNA fragments containing the *env* gene of SIVmac239 or Δ5G were isolated by digesting the mutated plasmids with BamHI and SmaI and were cloned into the SmaI- and BamHI-digested vaccinia virus vector plasmid pNZ68K2. To transfer the *env* gene from a recombinant plasmid to WRvv, the standard homologous recombination method using CV-1 cells was performed. Env expression in the recombinant vaccinia virus was confirmed by immunoprecipitation. The function of Env was confirmed by CD4- and CCR5-dependent fusion activity. The recombinant Env-expressing vaccinia viruses obtained were propagated and titrated in CV-1cells. The two recombinant viruses were propagated with similar kinetics in CV-1 cells.

Expression of SU-expressing plasmids and Env-expressing vaccinia virus in vitro. CV-1 cells were transfected with equal amounts of the following SU-expressing plasmids: pJWSUmac239, pJWSUmacΔ5G, or the vector pJW4303. Secreted SU metabolically labeled with ^{35}S protein labeling mix (PerkinElmer, Boston, MA) in culture supernatant was concentrated, immunoprecipitated with plasma from SIVmac239-infected monkeys, and then analyzed by sodium dodecyl sulfate-polyacrylamide electrophoresis (SDS-PAGE) as described previously (40). To examine Env-expressing vaccinia viruses, CV-1 cells were infected with WRvvmac239, WRvvΔ5G, or WRvv at a multiplicity of infection of 10, metabolically labeled with ^{35}S protein labeling mix overnight, lysed, immunoprecipitated with plasma from SIVmac239-infected monkeys, and then analyzed by SDS-PAGE as described for the expression of SU-expressing plasmids.

Animals, immunization, and challenge. Twelve juvenile rhesus macaques from Myanmar or Laos that were seronegative for SIV, simian T-cell lymphotropic virus, B virus, and type D retroviruses were used. As the polymorphism of major histocompatibility complex (MHC) genes influenced cellular immune responses against SIV/HIV infection, MHC II haplotypes and alleles of the macaques were determined (data not shown). All animals were housed in individual cages and maintained according to the rules and guidelines for experimental animal welfare stated by the National Institute of Infectious Diseases. As shown in Fig. 1, the 12 animals were divided into three immunization groups of four animals each: the SIVmac239 (wt)-Env immunization group (Mm0005, Mm0007, Mm0010, Mm0012), the Δ5G Env immunization group (Mm0001, Mm0002, Mm0003, Mm0009), and the vector control immunization group (Mm0004, Mm0006, Mm0008, Mm0011). All animals were inoculated with 1 mg of plasmid DNA in 1 ml of saline, one into each quadriceps femoris at 0, 4, and 8 weeks after the initial prime immunization (weeks p.p.). The boost consisted of 5×10^7 PFU of vaccinia virus in 1 ml of phosphate-buffered saline (PBS), administered in two 0.1-ml intradermal inoculations, one into the skin of each femur, and two 0.4-ml inoculations, one into each quadriceps femoris at 21 weeks p.p. All animals were

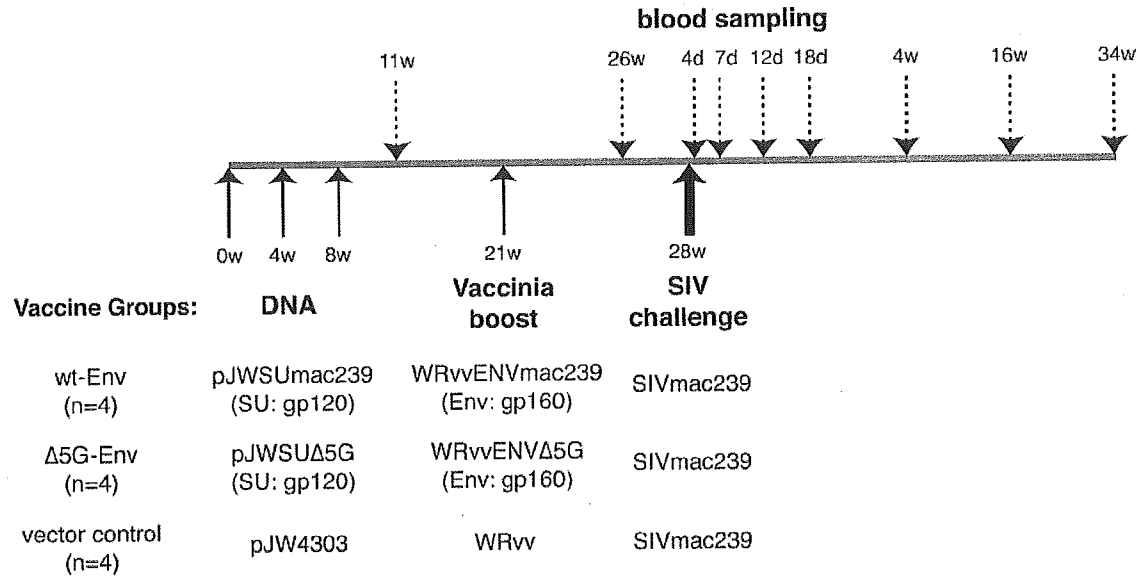

FIG. 1. Outline of immunization, challenge infection, and blood sampling. Twelve juvenile rhesus macaques were divided into three immunization groups of four animals each: the wt-Env immunization group (Mm0005, Mm0007, Mm0010, and Mm0012), the Δ5G Env immunization group (Mm0001, Mm0002, Mm0003, and Mm0009), and the vector control immunization group (Mm0004, Mm0006, Mm0008, and Mm0011). Animals were inoculated with a DNA vaccine (pJWSUmac239 for the wt-Env vaccine group, pJWSUΔ5G for the Δ5G Env vaccine group, and pJW4303 for the vector control group) at 0, 4, and 8 weeks p.p. The boost vaccine consisted of vaccinia virus (WRvvENVmac239 for the wt-Env vaccine group, WRvvENVΔ5G for the Δ5G Env vaccine group, and the WR strain for the vector control group) administered at 21 weeks p.p. All animals were challenged with 10 $TCID_{50}$ of SIVmac239 intravenously at 28 weeks p.p. w, weeks; d, day.

challenged with 10 50% tissue culture infective doses ($TCID_{50}$) of SIVmac239 intravenously at 28 weeks p.p.

Viral load measurement. To monitor SIV infection, the plasma viral load was measured by the real-time-PCR method described previously (36). Viral RNA was isolated from plasma from the infected animals using a commercial viral-RNA isolation kit (PE Applied Biosystems, Urayasu, Japan). SIV *gag* RNA was amplified and quantified using a commercial RNA reverse transcription (RT)-PCR kit (TaqMan EZ RT-PCR; PE Applied Biosystems) with the two *gag* primers, namely, the forward primer 1224F (5′-AATGCAGAGCCCCAAGAA GAC-3′), the reverse primer 1326R (5′-GGACCAAGGCCTAAAAAACCC-3′), and TaqMan probe 1272T (6-carboxyfluorescein-5′-ACCATGTTATGGCC AAATGCCCAGAC-3′-6-carboxymethylrhodamine). Purified viral RNA (10 μl) was reverse transcribed and amplified in a MicroAmp optical 96-well reaction plate (PE Applied Biosystems) according to the manufacturer's instructions and with the following thermal cycle conditions: 1 cycle of three sequential incubations (50°C for 2 min, 60°C for 30 min, and 95°C for 5 min) and then 50 cycles of amplification (95°C for 5 s, 62°C for 30 s) in a 7000 Prism sequence detection system (PE Applied Biosystems). In vitro RNA transcripts were quantified by optical density at 260 nm (OD_{260}) measurement and branched DNA assay for SIV viral RNA (Bayer Diagnostics, Tarrytown, N.Y.). RNA equivalent to 10 to 10^7 copies per reaction was used as the standard for each assay. The detection sensitivity of plasma viral RNA using this method was 1,000 copies/ml.

Flow cytometry. CD4 depletion was monitored by measuring the percentage of $CD4^+$ T cells, memory cells (CD29 high $CD4^+$) T cells (48) in PBMCs. PBMC samples were purified from a citrate anticoagulant containing blood using standard Ficoll-Hypaque gradient centrifugation. For flow cytometry, 2×10^5 PBMCs were reacted with fluorescein isothiocyanate or phycoerythrin-labeled antibodies (anti-human CD4, Nu-Th/I [Nichirei, Tokyo, Japan]; anti-human CD8, Leu2a [Becton Dickinson, San Jose, CA]; anti-human CD29, 4B4 [Coulter, Miami, FL]; anti-monkey CD3, FN-18 [Biosource, Camarillo, CA]; and anti-human CD20, Leu16 [Becton Dickinson, San Jose, CA]) as previously described (36, 37, 48).

Peptides. Overlapping peptides were synthesized by Emory University, Microchemical Facility, Winship Cancer Center (Atlanta, GA.). All SIVmac239 viral proteins except Env, Gag, Pol, Vif, Vpr, Vpx, Tat, Rev, and Nef were covered by consecutive 20-mer peptides overlapped by 12 amino acids. Env of SIVmac239 was covered by 72 consecutive 25-mer peptides overlapped by 13 amino acids. Peptides were dissolved in PBS with 10% dimethyl sulfoxide (Sigma Chemical, St. Louis, Mo.).

rSeV. Recombinant Sendai viruses (rSeV) expressing SIVmac239 Gag, SU, or Δ5G SU were used to infect herpesvirus papio-transformed B-lymphoblastoid cell lines (B-LCLs) to prepare autologous B-LCLs presenting these viral antigens. rSeV Gag expressing unprocessed SIVmac239 Gag and p55 (22, 23) and rSeV SU and rSeV/Δ5G SU expressing wt SU and Δ5G SU were constructed as described previously (52) and were also used to infect autologous B-LCLs.

Anti-SIV ELISA. A 1:100 dilution of each plasma sample in PBS (pH 7.4) containing a blocking reagent (Dainippon Seiyaku, Osaka, Japan) was assayed for SIV-specific antibody by using a standard enzyme-linked immunosorbent assay (ELISA) technique with 96-well plates precoated with SIVmac239 virion lysate. The OD_{492} was measured using a microplate reader (range of absorbance with linearity, 0 to 3.0; Tecan Japan, Tokyo, Japan) and utilized as a relative measurement of the antibody titer.

ELISPOT assay. Virus-specific $CD4^+$ T cells and $CD8^+$ T cells in PBMCs were measured using a monkey γ-IFN ELISPOT assay kit (U-CyTech, Utrecht, The Netherlands).

Cryopreserved PBMCs were thawed and cultured overnight in R-10 medium (RPMI 1640 [Sigma] supplemented with 10% heat-inactivated, defined fetal bovine serum [HyClone, Logan, Utah], 55 μM 2-mercaptoethanol, 50 U/ml penicillin, and 50 μg/ml streptomycin). PBMCs were subjected to the depletion of $CD4^+$ cells with magnet beads coated with anti-human CD4 Ab (Dynal ASA, Oslo, Norway) or subjected to the depletion of $CD8^+$ cells with magnet beads coated with anti-human CD8 Ab (Miltenyi Biotec, Bergisch Gladbach, Germany). Depletion of $CD4^+$ or $CD8^+$ cells from PBMCs was confirmed by flow cytometry. Using this depletion method, more than 95% of $CD4^+$ or CD8 cells were removed from PBMCs. These PBMCs were used for ELISPOT assay for virus-specific $CD8^+$ T cells and virus-specific $CD4^+$ T cells. Virus-specific stimulation of T cells was performed with autologous B-LCLs pulsed with pooled peptides for Pol, Vif, Vpx, Vpr, Tat, Rev, and Nef or B-LCLs infected with an rSeV for Gag, wt Env, and Δ5G Env. B-LCLs were incubated with pooled peptides corresponding to each viral protein at a final concentration of 2 μg/ml or infected with rSeV at a multiplicity of infection of 10 at 37°C overnight. Peptide-pulsed or infected B-LCLs were inactivated with long-wave UV irradiation (19) in the presence of 10 μg/ml psoralen (Sigma) for 10 min at a distance of 3.5 cm from a UV light, washed three times with R-10, and then used as stimulators in an ELISPOT assay. $CD4^+$ or $CD8^+$ cell-depleted PBMCs were cultured with these stimulators in an anti-γ-IFN Ab-coated ELISPOT plate (U-CyTech) overnight according to the protocol for the kit. Spots on the ELISPOT plate were imaged using an Olympus model SZX12 microscope